Environmental Research Plan
of the German Federal Ministry for the Environment,
Nature Conservation and Nuclear Safety

Protection of the Atmosphere

Executive Summary of Research Report No. 297 41 132

Statistical Analyses for the purpose of an early Detection of Global and Regional Climate Change due to the Anthropogenic Greenhouse Effect

by

Dr. Jürgen Grieser, Dipl.-Met. Tim Staeger
and Prof. Dr. Christian-Dietrich Schönwiese

University Frankfurt/Main, Institute for Meteorology and Geophysics
Working Group Meteorological Environment Research/Climatology

Working Group Leader

Prof. Dr. Christian-Dietrich Schönwiese

BY ORDER OF
THE FEDERAL ENVIRONMENT AGENCY

February 2000

The research-plan underlying this report was supported by the German Federal Minister for the Environment, Nature Conservation and Nuclear Safety. The responsability for the content of this publication rests with the authors.

1 Introduction

The assumption that mankind is able to have an influence on global or regional climate, respectively, due to the emission of greenhouse gases, is often discussed. This assumption is both very important and very obscure. In consequence, it is necessary to clarify definitively which meteorological elements (climate parameters) are influencend by the anthropogenic climate impact, and to which extent in which regions of the world. In addition, to be able to interprete such an information properly, it is also necessary to know the magnitude of the different climate signals due to natural variability (for example due to volcanic or solar activity) and the magnitide of stochastic climate noise. The usual tool of climatologists, general circulation models (GCM) suffer from the problem that they are at least quantitatively uncertain with regard to the regional patterns of the behaviour of climate elements and from the lack of accurate information about long-term (decadal and centennial) forcing. In contrast to that, statistical methods as used in this study have the advantage to test hypotheses directly based on observational data. So, we focus to the very reality of climate variability as it has occurred in the past.

We apply two strategies of time series analyis with regard to the observed climate variables under consideration. First, each time series is splitted into its variation components. This procedure is called 'structure-oriented time series separation'. The second strategy called 'cause-oriented time series separation' matches various time series representing various forcing mechanisms with those representing the climate behaviour (climate elements). In this way it can be assessed which part of observed climate variability can be explained by this (combined) forcing and which part remains unexplained.

2 Structure-oriented time series separation

The aim of this part of the study is to find out - preliminarily without asking for reasons - which climate variable components have experienced which significant change in the past. In the following subsection (2.1) the data base used for this analysis is presented. Within the subsequent subsection (2.2) an outline of the analysis technique is given. Finally, in the last subsection (2.3) the most important results are summarized. The cause-oriented analysis follows in section 3.

2.1 Data basis

In order to investigate long-term climate variations we prefer climate time series which cover a period of at least 100 years (centiennial variability). In order to eliminate the pronounced but partly chaotic weather phenomena we use only monthly data (monthly averages or, in case of precipitation, monthly totals). Data arranged in classes (ordinal scaling) like cloud coverage or wind intensity are not appropriate for such an analysis.

Table 1: Climatological time series data base (monthly if not indicated otherwise) as used in this study (G = global, NH = northern hemisphere, SH = southern hemisphere, E = Europe, D = Germany).

Data from station network					
Climate element	Region	Number	Period	Source	Abbrev.
Temperature, averages	D	9	1899 - 1998	DWD[1]	Te9
Temperature, Min.[2]	D	9	1899 - 1998	DWD[1]	Mi9
Temperature, Max.[2]	D	9	1899 - 1998	DWD[1]	Ma9
Humidity[3]	D	9	1899 - 1998	DWD[1]	Da9
Precipitation (totals)	D	9	1899 - 1998	DWD[1]	Ni9
Precipitation (totals)	D	81	1896 - 1995	[14]	Ni81
Temperature, averages	EU	41	1891 - 1990	[14]	Te41
Area-weighted data					
Temperature, averages	D	1	1798 - 1897	[13]	De3
	D	1	1898 - 1997		
	D	1	1798 - 1997		
Temperatur, averages	G	1	1899 - 1998	[10]	Gl3
	NH	1	1899 - 1998		
	SH	1	1899 - 1998		
Grid-point data					
Temperature, averages	E	52	1899 - 1998	[12]	Te52
Precipitation (totals)	E	83	1899 - 1998	[7]	Ni83
Mean sea level pressure	E	44	1896 - 1995	[1]	Dr44

In detail, three types of climate variable time series are analysed. First, we use time series related to a station network and tested for homogenity [14, 13, 16]. Depending from station density and representativeness of the considered climate variable in space, it is possible to characterize also the regional peculiarities of climate variability. However, due to some serious lack of such homogeneous time series, additionally grid-point-related data sets are used. The third type are area-related time series, i.e. global or hemispheric temperature averages, respectively, including also a 200 years temperature time series representing the area of Germany. An overview of all climate time series used is available from table 1.

[1] Deutscher Wetterdienst (German Weather Service)

[2] mean daily minima or maxima, respectively

[3] mean daily water vapour pressure

2.2 Method of analysis

The aim of 'structure-oriented time series separation' is to detect all variation components included in the time series under consideration and to discern these components from random noise. To realize this strategy we define any time series $x(t), x =$ climate element, $t =$ time, as a sum (superposition)

$$x(t) = a + t_r(t) + s(t) + l(t) + e(t) + h(t) + n(t) \tag{1}$$

with the components

a average
$t_r(t)$ trend (linear or progressive or degressive),
$s(t)$ seasonal component, i.e. annual cycle (constant or varying),
$l(t)$ episodic component (low-frequent without trend, polynomial structure),
$e(t)$ extreme events (differing significantly from a random-like frequency distribution),
$h(t)$ harmonic-cyclical component(s) excluding annual cycle,
$n(t)$ noise.

Each of these components can be exactly specified by mathematical equations as shown in the following.

(a) The trend can be approximated by

$$t_r = a_k + b_k\ t^k, \quad k = 1, 2, 3, 4, 5 \tag{2}$$

where a, b are the regression coefficients and k is power (here restricted to $k \leq 5$). Seven cases can be discerned: no (significant) trend, positive or negative linear trend, positive or negative progessive trend, and positive or negative degressive trend.

(b) The seasonal component can be expressed by

$$s_j(t) = d_j(t) \cos\left(2\,\pi \frac{j}{12}\,t\right) + e_j(t) \sin\left(2\,\pi \frac{j}{12}\,t\right) \text{ mit } j = 1, 2, 3, 4, 5, 6 \tag{3}$$

allowing 6 harmonic subcomponents of the annual cycle existent within the monthly data. As far as the change in time of this seasonal component is concerned, we use the expression

$$\begin{aligned} d_j(t) &= d_{j,0} + d_{j,1}\,t + d_{j,2}\,t^2 = \sum_{k=0}^{2} d_{j,k}\,t^k \\ e_j(t) &= e_{j,0} + e_{j,1}\,t + e_{j,2}\,t^2 = \sum_{k=0}^{2} e_{j,k}\,t^k, \end{aligned} \tag{4}$$

which is able to describe slow changes of this component.

(c) The episodic (low-frequent) component is described by means of polynomial equations of the form $l(t) = a_0 + \sum_k a_k t^k$ under the restriction $k \leq 5$. Note that this component represents neither a trend nor harmonic cyles but a behaviour which may imply relative extrema with wave number ≤ 2.

(d) In contrast to the usual consideration we define extreme events to be time series values showing a distance from the time-dependent expected time series value which exceeds significantly a specified random threshold. It can be assumed that there exist special reasons for the occurrence of such extreme events.

(e) If the time series components defined so far are substracted from the original time series, possible harmonic-cyclical components can be searched for by means of a periodogram analysis [15]. We use the Anderson-Darling test [15] in respect to white noise of the time series and, subsequently, test each maximum periodogram value in respect to a significant deviation from white noise.

(f) If all significant components detected in the time series under consideration are successfully substracted from the original time series, the residuum should represent stationary random noise. In case of Gaussian distributed variables it is sufficient to test stationarity in respect to average, variance, and autocorrelation. In consequence, deciding about Gaussian or non-Gaussian data distribution, we use the Kolmogoroff-Smirnoff test [15]. Then, the time series is subdivided into two subperiods of equal length, the related values of average, variance and autocorrelation are computed and tested in respect to a significant or non- significant difference. This leads to the detection of instationarities but is not a exhaustive procedure; that means if no instationarities are detected it cannot be concluded that they are really absent.

The tests in respect to average or variance stationarity are also performed using the time series of the different months of the year (time series of January values, February values and so on). Furthermore, for every of these month-related time series the year of the occurrence of extreme values (maxima and minima) are determined. This leads allows to detect possible instationarities also in these extreme values and to compare the results with those based on average and variance analysis. In this way some insight arises whether the extreme value behaviour of the time series under consideration is a consequence of the time- dependent behaviour of average or variance, respectively, or due to some additional dynamics.

Due to the fact that the technique used here for the separation of the time series variation components is only asymptotically orthogonal, the assessment of any components depend from the previous separation of the other components. For example, on the one hand, extreme events which are not separated may lead to a wrong assessment of the trend, or in other words: The trend value computed will be different with and without extreme events. On the other hand, extreme events can only realistically be detected if a possible trend is taken into account. This is why we use a successive strategy of analysis where, in the first guess, preliminary results are obtained, step by step corrected by the later results.

In detail, in the first step, the analysis starts with a selective regression where all possible seasonal and trend components are correlated with the original time series. If the relatively most significant component detected fulfills also a statistically defined threshold, it is separeted from the original time series via regression and the technique of selective regressions starts again. In the case, that in the second step in the same way an additional significant component is detected, a multiple regression based on these first two components detected leads to an improved assessment. This procedure comes to an end if no additional significant components can be detected. Then, the residuum time series is analysed in respect to its episodic components. The first guess of this analysis is the polynom of the largest order which is both statistically significant and explains significantly more variance then the other possibly signifcant low- order polynoms. Then, in the next step extreme events are looked for. This is done in the way that successively those values are subtracted from the residuum time series which show the relatively largest deviation from the average, under the presupposition that - as a conequence of the estimated frequency distribution - these values should not be likely to occur in a time series of defined length by random. The extreme events detected and subtracted in this way are substituted by values which coincide randomly with the residuum frequency distribution. It appears that this overall procedure needs only a few steps to converge against a robust assessment of the trend, seasonal, and episodic components. The residuum time series obtained at this step of the analysis are analysed in respect to possible harmonic-cyclical components. Finally, the residuum obtained in this very last step is tested against random noise. For comparison, this test is also perfomed using the original time series. In order to judge the time-dependent behaviour of variance, for each time series under consideration the related time series of moving standard deviations is computed. Moving standard deviation is preferred in comparison to moving variance because the former time series variable is χ-distributed and the latter χ^2-distributed: The χ-distribution converges more quickly to the Gausssian distribution. The strategy described above is also applied on the time series of moving standard deviations.

2.3 Results

Table 2a reveals the number of detected trends for all seven types of trends (see section 2.2) and for all data time series considered (see listing in table 1). Both the global mean and the (northern and southern) hemispheric mean temperature data (G3) show a positive progessive trend (increasing with time). In case of the mean German temperature data (D3) and the period 1798-1897 no trend is indicated, however, a positive linear trend for 1898-1997 and reasonably a positive progressive trend for the total period 1798-1997. Most of the 9 certainly homogeneous time series of mean, maximum, and minimum temperature from Germany (Te9, Mi9, Ma9) reveal positive progressive trends whereas in case of the related humidity (Hu9) and precipitation (Pr9) time series no significant or positive linear trends arise. A closer look on precipitation at 81 German stations (probably instead of certainly homogeneous) leads to an outstanding West-East structure where in the East no

Table 2: Number of trends detected in a) climate element time series and b) related moving standard deviation time series. The abbreviations are as follows: p = progressive, l = linear, d = degressive; for abbreviations of data sets (Te9 etc.) see Table 1.

a)	negative			none	positive		
	p	l	d		d	l	p
Te9						1	8
Mi9							9
Ma9						2	7
Pr9				4		3	2
Hu9				4	1	3	1
G3							3
D3				1		1	1
Pr81	1	2		24		26	28
Te41	1			6	2	29	3
Te52	5			5	4	24	14
Pr83	7	6		31	1	18	20
SLP44	3	7	5	27			2

b)	negative			none	positive		
	p	l	d		d	l	p
Te9				7			2
Mi9		1		5			3
Ma9				6			3
Pr9				3		5	1
Hu9	2			6		1	
G3	2			1			
D3		2		1			
Pr81				50		24	7
Te41	6			35			
Te52	23	5	1	21		2	
Pr83	9	1		34	2	30	7
SLP44	3			36		2	3

trends are dominating, see Fig. 1a. This effect cannot be detected in the related gridded data (Pr83), see Fig. 1b, due to a poor resolution in space. Instead, Fig. 1b points to a significant precipitation decrease in the Mediterranean area contrasted by a significant precipitation increase in Northern and Eastern Europe. Related to the European temperature data, from station network (Te41) or gridded (Te52), respectively, positive linear trends are dominating. A significant change of sea level pressure (SLP44) appears only in South-Eastern Europe characterized by negative trends (linear and non-linear). Table 2b specifies the trends detected in the related moving standard deviation time series where less significant trends are detected compared to the climate element time series themselves. Nevertheless, it can be stated that in case of temperature negative and in case of precipitation positive trends prevail. It is possible, however, that the temperature standard deviation trends are influenced by improving measurement accuracy. So, these trends may be an artefact and not due to real climate change. The episodic component is not discussed here because, on average, it cannot explain more than 2.5% of variance, except Gl3 (global and hemispheric mean temperature data).

In Table 3 the number of time series is indicated where a change of the seasonal component (annual cycle) is detected. In overview, it can be stated that a change of the shape of the seasonal component (due to a change of superimposed harmonics) is most frequent. A change of the amplitude is less frequent and a change of the phase is even more seldom. As an example of a change of the phase (basic cycle), Fig. 2 specifies the spatial pattern of this change in respect to temperature as observed at European stations (Te41). Similarily, Fig. 3 specifies the spatial pattern of the change of amplitudes with regard to the gridded European temperature (Te52).

Table 3: Number of climatic time series where a change of amplitude (A) or phase (φ) is detected, concerning the basic cycle, the harmonics and their superposition of the seasonal component (annual cycle). Heavy numbers indicate that the 90% confidence level is exceeded.

	Basic cycle		Harmonics		Superposition	
	A	φ	A	φ	A	φ
Te9	**8**	0	0	0	**8**	0
Mi9	1	0	0	0	1	0
Ma9	**5**	0	0	0	**5**	0
Pr9	**7**	**3**	0	0	**7**	**3**
Hu9	**4**	2	2	2	**4**	2
G3	**2**	**2**	**2**	**2**	0	0
D3	1	1	1	1	1	0
Pr81	**57**	**26**	**16**	**14**	**47**	**13**
Te41	**29**	**19**	**18**	**18**	**24**	3
Te52	**30**	**9**	**24**	8	**10**	2
Pr83	**52**	**18**	10	10	**52**	11
SLP44	**35**	**13**	**17**	**12**	**31**	3

Table 4: Number and type of extreme events detected within two subperiods of equal length and significance p of the difference of these numbers.

	Total	Minima			Maxima		
		1. Subp.	2. Supp.	p [%]	1. Subp.	2. Subp.	p [%]
Te9	69	38	31		0	0	
Mi9	103	50	53		0	0	
Ma9	27	19	8	95	0	0	
Pr9	52	0	0		28	24	
Hu9	6	0	0		4	2	
G3	5	2	0		3	0	
D3	23	11	12		0	0	
Pr81	444	0	0		186	258	99.9
Te41	208	73	127	99.99	3	5	
Te52	231	116	74	99	32	9	99.9
Pr83	405	1	4		137	263	99.99
SLP44	137	13	31	99	37	56	95

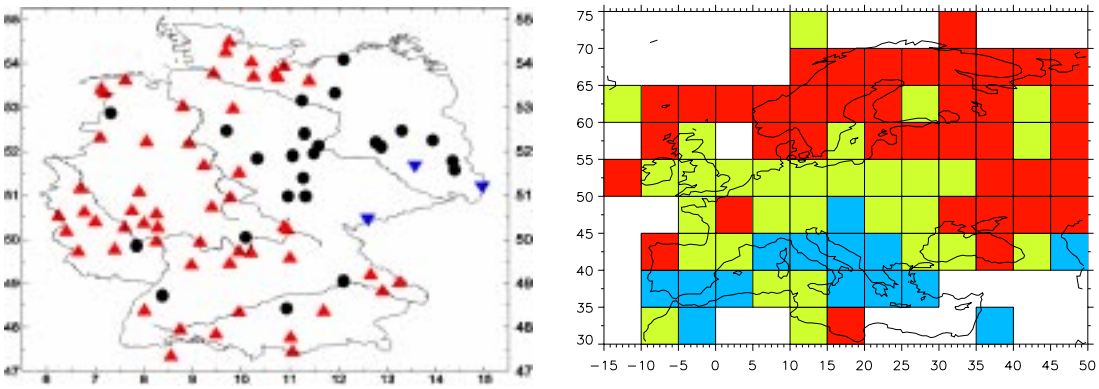

Figure 1: Sign of precipitation trends detected a) in data from German stations and b) in European gridded data. In Fig. 1a circles mean no, blue triangles positive and red triangles negative trends. In Fig. 1b blue means positive, red negative and grey shading no trend (white areas: no data)

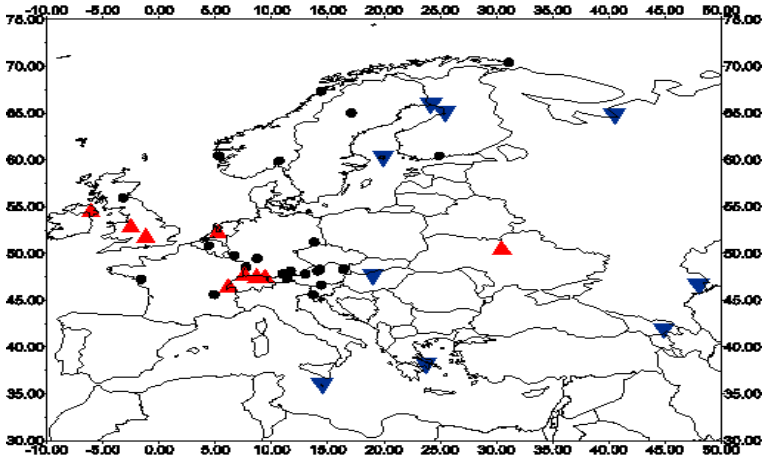

Figure 2: Change of the phase of the basic cycle of the seasonal component (annual cycle) of temperature in Europe. Circles mean no significant, blue triangles significant positive and red triangles significant negative change.

As far as extremes are concerned, the analysis of German and European temperature data reveals almost exclusively negative extreme events, see table 4, almost all in winter, see table 5. In contrast to that, precipitation extreme events are almost exclusively positive prevailing in summer. Extreme cold winter months, significantly not fitting the random hypothesis of time series analysis, evidently appear during high pressure blocking weather situations. Table 5 points to the fact that, in Europe, their frequency has increased significantly in the later subperiod when compared with the earlier if the total period is divided into two subperiods of equal length. This confirms our concept to analyse extremes and trends separately, that means to eliminate extremes before a trend analysis.

Although an analysis of precipitation in Germany (Pr81) shows that most of the extreme events appear in summer, it is reasonable to look also and particularly on winter, because

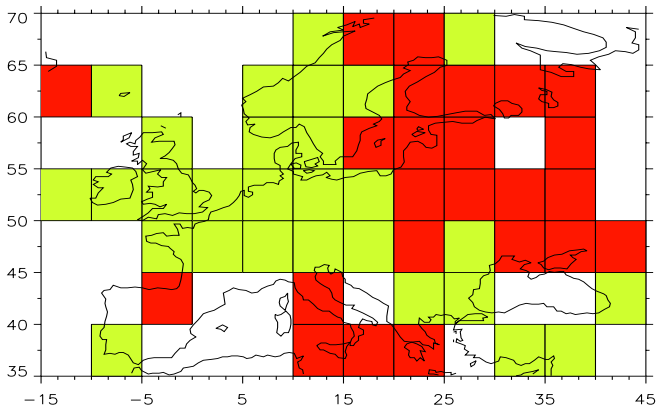

Figure 3: Change of the amplitude of the basic cycle of the seasonal component (annual cycle) of temperature in Europe. Red means positive (increase), grey no change (white areas: no data).

Table 5: Number of extreme events in the different months of the year detected in European temperature (Te41, only minima) and German precipitation (Pr81, only maxima) within two subperiods of equal length and significance p of the difference of these numbers.

	Temperature minima (Europe)			Precipitation maxima (Germany)		
	1. Subp.	2. Subp.	p [%]	1. Subp.	2. Subp.	p [%]
Jan.	18	47	99.98	1	6	93.75
Febr.	44	77	99.83	5	24	99.97
March	1	1		0	11	99.95
April	0	1		4	3	
May	1	0		10	17	
June	0	0		25	21	
July	0	0		57	58	
Aug.	1	0		47	47	
Sept.	0	0		14	17	
Okt.	0	1		32	17	97.78
Nov.	2	1		2	9	96.41
Dec.	9	4		2	15	99.88

the most pronounced change of the extreme event behaviour appears in winter. For instance, the number of extreme winter precipitation events has significantly decreased in October but significantly increased in the months November to March.

As a significant harmonic component a 92.3 months (7.7 yr) cycle is detected in European temperature, in Germany particularily in averages and maximum data. The same cycle is also existent in the North Atlantic Osillation (NAO) [19].

In summary, all climate variables under consideration show their specific structures as revealed by our time series analysis. However, they are most pronounced in case of temperature and precipitation. In addition to positive temperature trends (global and regional warming), special attention should be directed to precipitation where an increase of mean totals, standard deviation, and - separated from other variability - winter extreme events is evident. There is an important link of these phenomena to ecological and economic affairs.

3 Cause-related time series separation

Now, the question has to be answered which causes may have led to the climate time series variation structure as described in section 2. Similar to that section, first the data basis is introduced (section 3.1). Subsequently the method of analysis is discussed (section 3.2) and the results are presented (section 3.3). Thereby, the aim is to assess how much of observed climate variance may be explained by each of the time series representing the causes, including the magnitude of the related climate signals.

3.1 Data basis

Due to the intention of this section to detect cause-effect relationships, forcing (cause) and climate (effect) data are discerned. For this purpose, a pool of potential forcing parameter data time series is taken into account to be related to climate variable time series. The following potential forcing is used:

- Atmospheric concentrations of greenhouse gases GHG (carbon dioxide equivalents CO_2E) increasing due to human activities where it is supposed that (by physical reasons in the context of the related heat rate anomalies) the temperature reponse is logarithmically proportional to this forcing; so this input is logarithmic ($ln CO_2E$).
- Tropospheric sulfate aerosol concentrations SUL (column density) supposed to be directly proportional to the anthropogenic emission of sulfur dioxide (SO_2) [2] where in this case the first three time-related principal components (see section 3.2) are used as an input;
- Southern Oscillation index (SOI) representing the El Niño / southern oscillation mechanism ENSO (data provided by the Climatic Research Unit, University of Norwich, UK);
- Explosive volcanic activity VOL represented by the first three time-related principal components of volcanogenic heat rate anomalies adopted from Grieser [3];
- Solar activity SOL represented alternatively by sunspot relative numbers and related hypothetical variations of the solar extraterrestrial insolation adopted from Lean et al. [11];

- Index of North Atlantic Oscillation NAO which provides some information about the atmospheric circulation types within the North Atlantic - European region [8, 9].

In order to take account for the inertia of the climate system all forcing parameter data time series listed above are used also in their 1 and 2 yr time lags, except CO_2E (due to outstanding autocorrelation).

In the following the climate variable time series representing the effects of forcing are listed up. Data also used in section 2 are marked by an asterisk *).

- Surface air temperature annual means, global and hemispheric averages 1899-1998 [10] *).
- Surface air temperature annual means 1868-1995, eight zonal average time series covering the whole globe (derived from [6]).
- Surface air temperature, annual and seasonal means 1894-1995, 80 area- related time series (each of equal area, 8 areas missing due to data gaps) covering the whole globe (derived from [10], area design from [5]).
- Sea level air pressure, annual and seasonal means 1900-1992, area arrangement as above, but only oceanic areas (62 time series), adopted from [17] (based on the Comprehensive Ocean Atmosphere Data Set COADS).
- Surface air temperature, Europe, annual and monthly means 1899-1998, gridded data $5° \times 5°$ (52 time series, adopted from [12] *).
- Sea level air pressure, Europe, annual and monthly means 1896-1995, gridded data [1] *).
- Precipitation, Europe, annual and monthly totals 1900-1998, gridded data as above [7] *).

3.2 Method of analysis

The purpose of analysis within this section is to find and to separate those forcing parameter time series which are significantly correlated with the climate variable time series under consideration and attribute the corresponding explained variance (producing related climate signals) to each of these selected relationships. Furthermore, the residuum climate time series are subdivided into two parts: residuum which implies some significant but unexplained variance and residuum which fulfills the statistical criteria of random noise (see section 2.2). This enables a detailed signal-to-noise analysis where the climate signals explained by any particular forcing (for example GHG) are related to the noise residuum.

Due to the fact that, with the exception of global or hemispheric mean temperature, all data sets represent variations in time and space (system of area-related or gridded

time series, respectively, data fields), within a preanalysis an EOF (empirical orhogonal functions) transformation was performed. So, for example, instead of 50 climate variable time series at 50 different grid-points one obtains 50 time-related principal components, ranked according to their explained variance:

$$z(x,t) = \sum_{j=1}^{m} \lambda_j EOF_j(x) PC_j(t) \quad , \tag{5}$$

where $z(x,t)$ is the original space-time related data field, transformed into m time-related principal components $PC_j(t)$ and a series of space-related principal components, called empirical orthogonal functions $EOF_j(x)$; details see references [4]. The factor λ_j is called eigenvalue and quantifies the weight (also the amount of variance) of the related principal component existent in the original climate data field. The EOF_j provides the information about the weight of the corresponding PC existent at the related point of space.

Using these statistical techniques, a successive regression enables to select from the pool of potential forcing parameter time series these ones revealing a significant correlation with the $PC_j, j = 1, \ldots, m$, which are the new substitutes of the climate data. In this context 'successive' means the following procedure.

- Computation of the linear correlation coefficients r between each of the forcing parameter time series $E_k(t)$ and the $PC_j(t)$ considered.
- The $E_k(t)$ revealing the most significant (threshold confidence level 95%) correlation is the first 'winner' $E_{w1}(t)$.
- The linear regression between $E_{w1}(t)$ and $PC_j(t)$ is computed.
- The resulting residuum $R_1(t)$ is the new climate data input.

This procedure is repeated until no more significant correlations remain. Finally, the forcing parameter time series $E_{Si}(t)$ selected in this way are related to each of $PC_j(t)$ representing the new climate variable via the multiple linear regression

$$\widehat{PC}_j(t) = a_0 + \sum_{i=1}^{l} a_i E_{Si}(t) \quad , \tag{6}$$

where a_i are the regression coefficients. So, one gets a relationship between $PC_j(t)$ and the significantly correlated forcing parameters which can be related to the original climatic data field using a retransformation into space coordiates via

$$z(x,t) = S_{anthr}(x,t) + S_{nat}(x,t) + R(x,t) \quad , \tag{7}$$

where S_{anthr} is the anthropogenically forced signal field and S_{nat} is natural. The unexplained residuum field $R(x,t)$ is analysed in the way as already described in section 2.2. That means, one looks particularly for trend and episodic (polynomial) components which

- if significantly existent - form the structurated part of R. The remaining part of R without structure is supposed (and tested) to form the random noise residuum (details see German report [4]). In consequence, one gets an information about a more or less reasonable selection of forcing parameters (some important missing?). Furthermore, testing the proportion between S_{anthr} and the noisy part of R, one gets an assessment of the anthropogenic climate signal-to-noise ratio and, in consequence, of the confidence level of the detection of the anthropogenic influence on climate.

Note that it is important in this context to consider all potential forcing of climate (anthropogenic and natural) to get a realistic assessment of climate noise.

If the ratio between the anthropogenic greenhouse forcing signal $S_{anthr,GHG}$ and the standard deviation of climate noise s_{noise} is denoted to be the detection variable $d(x,t)$, it is possible to compute the space-time related probability p of greenhouse (or other) induced climate change using the following equation

$$\begin{aligned} P\left(z \leq |d(x,t)|\right) &= erf\left(\frac{d(x,t)}{\sqrt{2}}\right) \quad , \\ with \quad erf(x) &= \frac{2}{\sqrt{\pi}} \int_0^x exp\left(-u^2\right) du \quad . \end{aligned} \tag{8}$$

The term '$erf(x)$' is the so-called error function which can be treated by numerical methods. Eq. (8) is applicable because the random noise residuum is Gaussian distributed.

3.3 Results

In the following, starting with global and hemispheric mean temperatures and proceeding towards gridded data from Europe, the results move from a global to a more and more regional scale (compare data basis, section 3.1).

Because some of the potential forcing mechanism parameter time series have a similar structure which hampers their separation in the statistical analysis (competing effects), different combinations of these forcing time series are used. Thereby it arises that especially greenhouse gases (GHG) and sulfate particles (SUL, both anthropogenic forcing) interfere with each other when the global gridded mean sea level air pressure field is considered. This is why in Table 6 which summarizes the signal analysis results, column 5 reveals the explained variance with and without (in parantheses) SUL forcing.

Table 6 shows that the total explained variance (TOT) decreases as the consideration proceeds from a large to small (regional) scales. The same holds for the anthropogenic GHG signal, very pronounced in case of temperature. This is due to the noise reduction effected by averaging. With regard to temperature and the GHG signal, this is again demonstrated in Fig. 4, contrasted by the ENSO signal which is of more regional relevance. It is worth noting that NAO is of more regional relevance, too, however, in this case with regard

Table 6: Percent of explained variance of the total signal (all forcing, TOT, based on multiple regression) and the individual signals (due to the particular forcing listed in column 1, GHG..., based on successive regression). The abbreviations are as follows: T = temperature, SLP = sea level pressure, P = precipitation, GA = global average, ZA = zonal averages (latitude bands), G = gridded data (index indicating number of grid-points); TOT = total sum of explained variance, GHG = greenhouse gases, SUL = tropospheric sulfate aerosol, VOL = volcanism, ENSO = El Niño / southern oscillation, SOL = solar activity, NAO = North Atlantic Oscillation, RS = structurated residuum, RN = noise residuum.

	Global				Europe		
	T, GA	T, ZA	T, G_{72}	SLP, G_{62}	T, G_{52}	SLP, G_{44}	P, G_{83}
TOT	79.7	51.0	38.8	29.1	21.3	27.8	13.2
GHG	59.9	35.7	19.0	0.5 (7.9)	7.6	0.6	3.5
SUL	3.1	0.2	3.2	9.6 (-)	1.5	3.5	1.4
VOL	6.0	6.7	4.0	5.1	0.8	2.0	1.1
ENSO	4.2	6.2	7.1	5.7	0.1	0.4	1.4
SOL	4.2	0.3	2.2	3.2	2.1	0.9	1.3
NAO	0.0	0.0	2.6	3.1	8.9	20.2	4.2
RS	-	-	7.1	7.6	10.5	3.8	3.8
RN	-	-	54.1	63.3	68.2	68.4	83.0

to Europe (see again Fig. 4). Moreover, the NAO signal entails a pronounced seasonal variation (Figure not shown, see detailed report in German [4]). All climate data sets analysed reveal a noise residuum component RN which is evidently much larger than in case of the structurated residuum RS. From this result it can be concluded that most important climate forcing is satisfactorily taken into account.

Concerning the magnitude of the related GHG forced temperature signals, Fig. 5b shows the analysis result based on a global data set of 72 subareas in the year 1995 (compared to 1894). Nearly all regions are characterized by a GHG forced warming up to approximately 1.7 K in the interior of the large continents of the northern hemisphere. The cooling amounting to - 0.1 to -0.3 K in the North Atlantic region may have something to do with with atmospheric circulation anomalies in connection with NAO or/and with a more intensive mixing of oceanic mixed layer waters.

Fig. 5a gives the answer to the region-related question whether the GHG signal is detected until the same year 1995 (SUL forcing neglected). The colours indicate the probability of this detection for confidence levels $> 90\%$. It is worth noting that the regions of maximum confidence do not coincide with the regions of maximum signal amplitude. Because of the fact, that not the signal alone but the signal-to-noise ratio decides whether such a signal is detected or not, it is possible that this detection succeeds at a high level of confidence in the regions where the overall climate variable standard deviation is rather small, for example in oceanic regions (small heat capacity, no orographic effects on atmospheric circulation). In detail, Fig. 5a shows that 47 from a total of 62 subareas indicate that

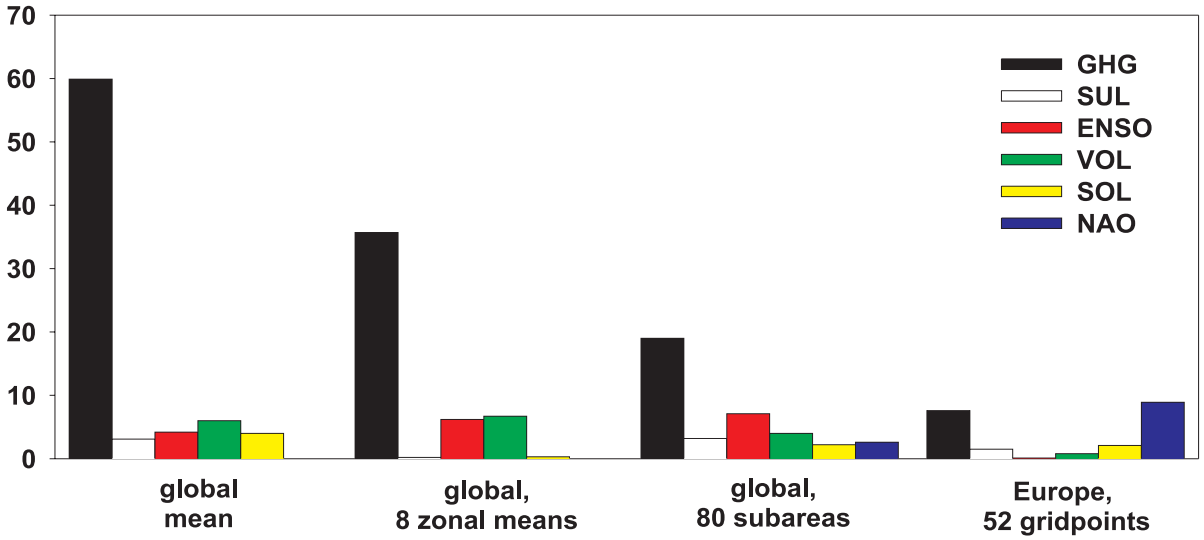

Figure 4: Explained temperature variance due to the indicated forcing (GHG, ...) based on the successive regressions as described in the text. From left to right scaling proceeds from global average to more regional scaling.

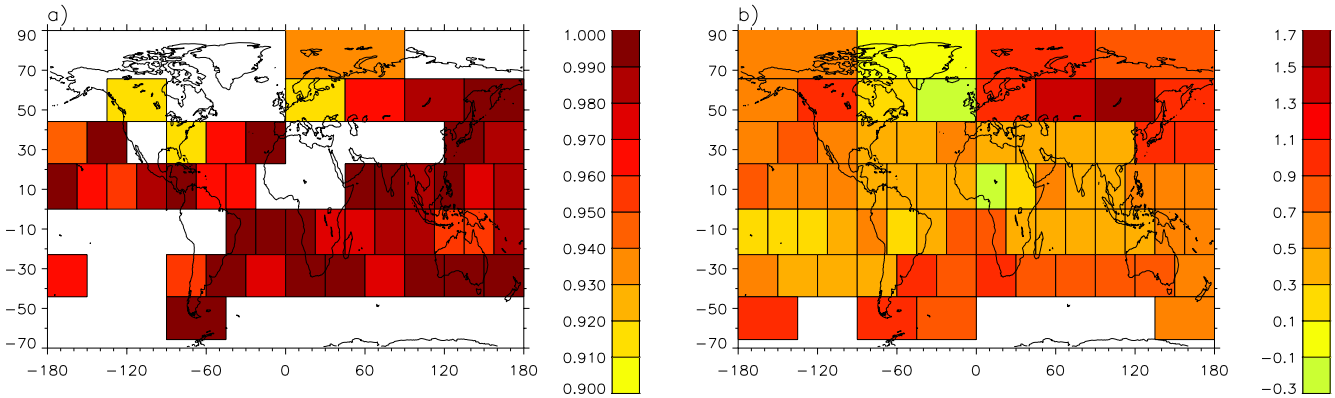

Figure 5: a) Probability p in percent that climate change in temperature (global,72 subareas considered) due to the anthropogenic greenhouse effect (GHG forcing) has taken place from the year 1894 to 1995; the colours specify confidence levels $> 90\%$. b) Related temperature signals in K (SUL forcing neglected).

the anthropogenic GHG signal is detected exceeding a confidence level of 90%; within 42 subareas the 95% and within 19 subareass the 99% level is exceeded. That means, the GHG signal is detected in the global regionally disintergrated temperature variations with a high degree of probability.

At this point it should be mentioned, that the probability for climate change with regard to the global mean temperature clearly exceeds the 99.9% significance level (in the year 1998), due to the large amount of explained variance (59.9%, see Table 6) and the distinct trend of the GHG-signal in contrast to the low noise.

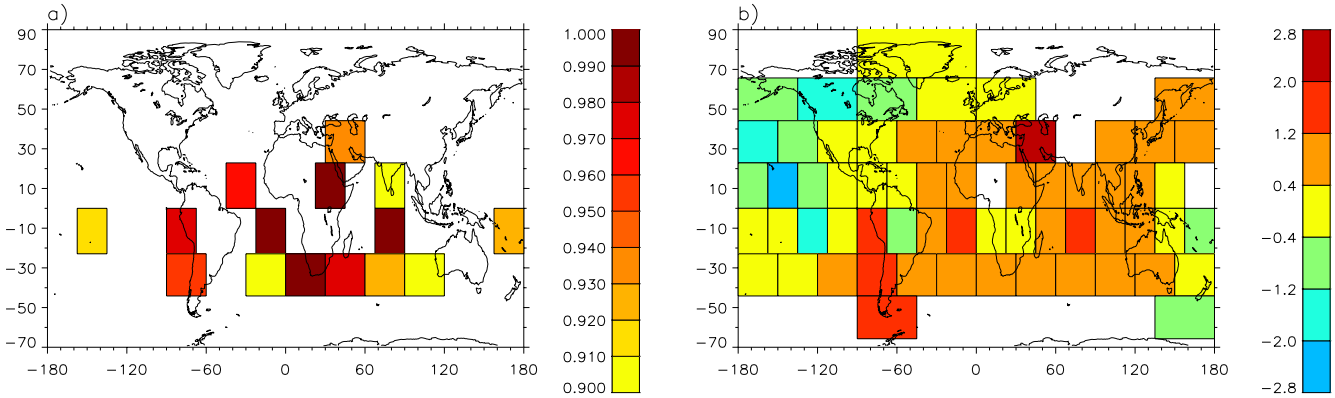

Figure 6: Similar to Fig. 5, but sea level pressure, 62 subareas, period 1902- 1992.

Similar to Fig. 5b, Fig. 6b specifies the GHG induced signals in mean sea level pressure (SLP), global consideration, 62 subareas (again SUL forcing neglected). The climatological interpretation, however, is problematical. Moreover, comparing Figure 5 with 6 and in coincidence with Table 6, the detection of the GHG signal in SLP data is much poorer than in temperature. Nevertheless, as revealed in Fig. 6a, related to the year 1992 within 15 from a total of 62 subareas the 90% level of confidence is exceeded, the 95% level in 8 subareas, and the 99% level in 4 subareas. This means, that also the sea level pressure analysis leads to a detection of the anthropogenic GHG signal at a high level of probability.

In Fig. 7b the GHG forced signal field as detected in the European temperature is plotted. As in case of the global analysis (see Fig. 5b) positive anomalies dominate where a maximum amplitude of approximately 1.7 K is reached in North Eastern Europe. Negative signals amounting to ca. -0.6 K at the maximum are found east of Iceland, coinciding well with the global analysis (see again Fig. 5b), and in the South Eastern part of Europe (Greece, Turkey). Again, the anthropogenic influence on climate is proved because this subresult of the detection analysis reveals within 11 from a total of 52 subareas that the 90% confidence level is exceeded, moreover in 4 subareas the 95% level (but nowhere the 99% level).

The signal results with regard to sea level pressure in Europe, see Fig. 8b, similar to the global scale (see Fig. 6b), are hard to interprete. As indicated in the analysis of explained variance, see Fig. 8a, the detection of the GHG signal is very restricted in this case. Only within two neighboured subareas (uppermost South Eastern region of Europe) a confidence level of 99% is exceeded; strange enough, in none of the other subareas any confidence level $> 90\%$ is exceeded.

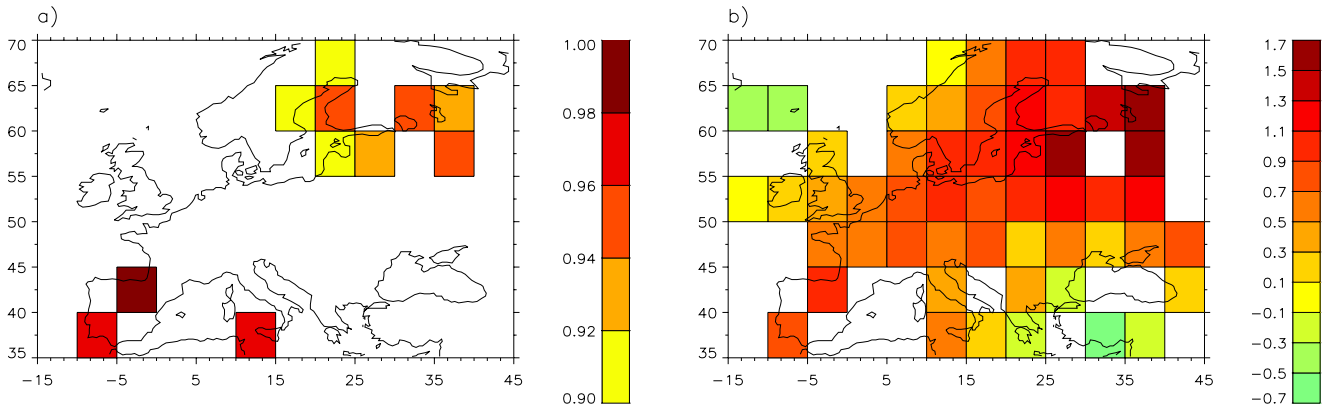

Figure 7: Similar to Fig. 5, but European temperature, 52 grid-points, period 1899-1998 (including SUL forcing).

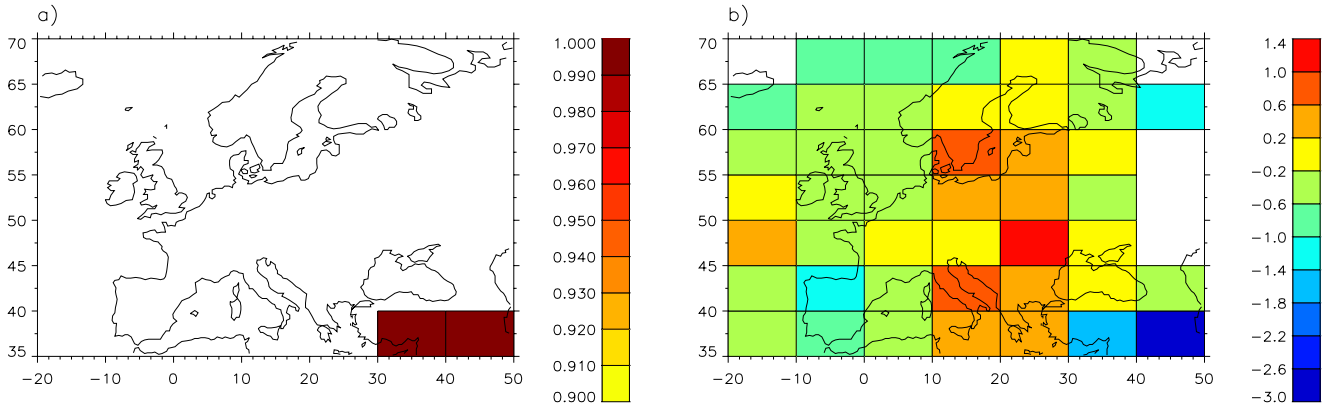

Figure 8: Similar to Fig. 5, but European sea level pressure, 44 grid-points, period 1896-1995.

The GHG forced European precipitation signal field shows a striking structure revealing positive anomalies in Northern and negative anomalies in Southern regions (see Fig. 9b). This coincides with the trend analysis performed in the context of the 'structure-oriented time series separation' (see section 2.3 and [16]) and the NAO forced signal field (not shown here; see detailed report in German [4]). Due to the very high contribution of noise to precipitation variations (see Table 6) the detection of the GHG forcing in European precipitation does not succeed (only within 2 subareas from a total of 83 the 90% confidence level is exceeded; this is statistically not significant).

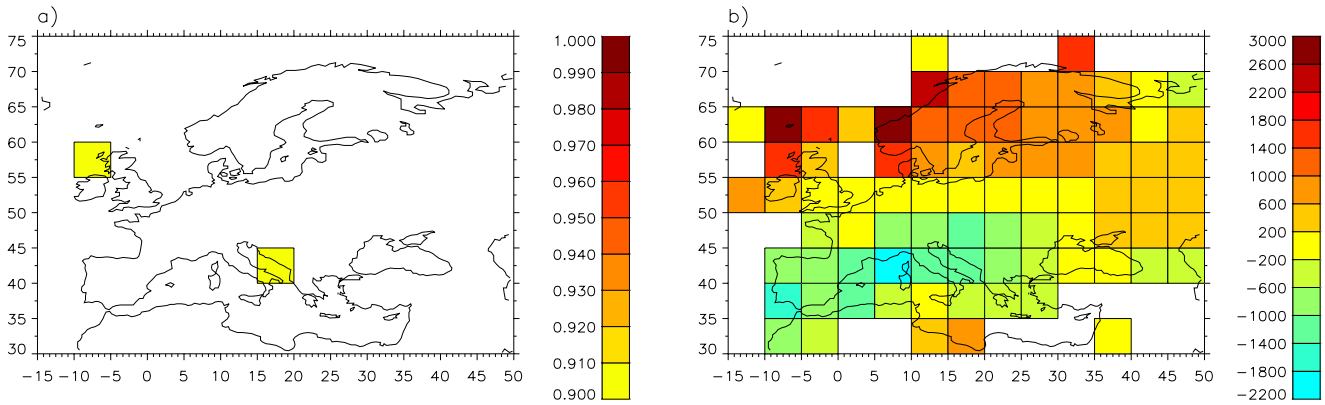

Figure 9: Similar to Fig. 5, but European precipitation, 83 grid-points period 1900-1998.

4 Outlook

In such a brief summary of our detailed analysis (as provided in our detailed German report [4]) only a rough overview of the methods and results can be given. However, we think it is obvious from this summary that the analysis methods evaluated in the context of this project and their application on climatological time series analyis was successful confirmed by a lot of results which should be of both scientific and public interest. It would be no problem to apply these methods also on other data sets, in particular on additional climate elements (parameters), in other regional design and on other time scales.

An extension of the 'structure-oriented time series deparation' could imply additional time series structures in the context of the successive selection strategy. In case of the detection of extreme events also non-Gaussian distributed quantities could be considered, for example special monthly precipitation distributions. As far as the residuum time series are concerned, they are supposed to represent linear stochastic processes; however, this is not necessarily the case. In some further research, therefore, more attention may be payed to the type of stochastic processes describing in an optimal way the residuum data. In consequence, this would improve also the detection of anthropogenic climate change (e.g. in case of precipitation).

An important information available by means of the 'structure-oriented time series separation' is the time-dependent probability that defined data thresholds are exceeded. In this way the effects of variations of average and variance in time can be incorporated in the analysis. (A special example is available from the detailed German report [4].)

The 'cause-related time series separation' may be improved by the incorporation of additional potential forcing mechanisms. In case of forcing parameter time series which have proven to be problematical such as SUL forcing (tropospheric sulfate aerosol), it would be reasonable to perform the analysis procedure again as soon as an improved parameter for this forcing can be provided. In addition, alternative parameterizations of identical forcing

mechanisms, for example volcanic or solar, may be tested with regard to their statistical properties in order to select the best approximation.

Another possibility for further research is the introduction of non-linear cause- effect relationships. This may be realized by the power of some forcing parameters or by sigmoidal functions. This type of relationships which implies a slow reaction in the beginning and a saturation effect near the end of the relation function is used by neural networks [18]. Mixed terms of influence parameters may take account for interactions between the different forcing mechanisms. Neural networks, already mentioned, can help to assess the degree of nonlinearity of cause-effect relationships. This leads also to an assessment of the maximum of variance which can be explained by these relationships.

These are only a few possibilities to come to further progress in the research where empirical-statistical analyses of climate variability are performed. No doubt, the problem to separate anthropogenic from natural forcing in observed climate variability, global and regional, we have addressed in this project and we may address in future research, is one of the most important problems in climatology.

References

[1] T. A. Basnett and D. E. Parker. Development of the Global Mean Sea Level Pressure Data Set GMSLP2. Climatic Research Technical Note 79, Hadley Center, Meteorological Office, Bracknell, 1997.

[2] R. J. Charlson, J. Langner, C. B. Leovy, and S. G. Warren. Pertubation of the nothern hemisphere radiative balance by backscattering from anthropogenic sulfate aerosols. *Tellus*, 43AB:152–163, 1991.

[3] J. Grieser and C.-D. Schönwiese. Parametrization of Spatio-temporal Patterns of Volcanic Aerosol Induced Stratospheric Optical Depth and its Climate Radiative Forcing. *Atmósfera*, 12:111–133, 1998.

[4] J. Grieser, T.Staeger, and C.-D. Schönwiese. Statistische Analysen zur Früherkennung globaler und regionaler Klimaänderungen aufgrund des anthropogenen Treibhauseffektes. Institutsbericht 103, Inst. f. Meteorologie u. Geophysik, Universität Frankfurt, 2000.

[5] J. Hansen and S. Lebedeff. Global trends of measured surface air temperature. *J. Geophys. Res.*, 92:13345–13372, 1987.

[6] J. Hansen, R. Ruedy, M. Sato, and R. Reynolds. Global surface air temperature 1995: Return to pre-Pinatubo level. *Geophys. Res. Lett.*, 23:1665–1668, 1996.

[7] M. Hulme, T. J. Osborn, and T. C. Johns. Precipitation sensitivity to global warming: Comparison of observations with HadCM2 simulations. *Geophys. Res. Letts.*, 25:3379–3382, 1998.

[8] J. W. Hurell and H. van Loon. Decadal variations in climate associated with the North Atlantic oscillation. *Climate Change*, 36:301–326, 1997.

[9] P. D. Jones, T. Jónsson, and D. Wheeler. Extension to the North Atlantic Oscillation using early instrumental pressure observations from gribraltar and South West Iceland. *International Journal of Climatology*, 17:1433–1450, 1997.

[10] P. D. Jones, T. M. L. Wigley, and K. R. Briffa. Global and hemispheric temperature anomalies - land and marine instrumental records. In T. A. Boden, D. P. Kaiser, R. J. Sepanski, and F. W. Stoss, editors, *Trends '93: A Compendium of Data on Global Climatic Change*, pages 603 – 608. Climate Monitor, 1994.

[11] J. Lean, J. Beer, and R. Bradley. Reconstrction of solar irradiance since 1610: Implications for climate change. *Geophys. Res. Lett.*, 22(23):3195–3198, 1995.

[12] D. E. Parker, P. D. Jones, C. K. Folland, and A. Bevan. Interdecadal changes of surface temperature since the late nineteenth century. *J. Geophys. Res.*, 99:14373–14399, 1994.

[13] J. Rapp. *Konzeption der statistischen Trendanalyse von Klimadaten und ihre Anwendung auf aktuelle Zeitreihen aus Europa bzw. Deutschland.* Dissertation, Inst. f. Meteorologie u. Geophysik, Universität Frankfurt/Main, 2000. in Vorbereitung.

[14] J. Rapp and C.-D. Schönwiese. *Atlas der Niederschlags- und Temperaturtrends in Deutschland 1891 - 1990*, volume 5 of *Serie B.* Frankfurter Geowissensch. Arbeiten, Frankfurt, 1996. 2. Aufl.

[15] R. Schlittgen and B. H. J. Streitberg. *Zeitreihenanalyse.* R. Oldenbourg Verlag, München, 5. edition, 1994.

[16] C.-D. Schönwiese and J. Rapp. *Climate Trend Atlas of Europe - Based on Observations 1891-1990.* Kluwer Academic Publishers, Dordrecht, 1997.

[17] T. Staeger. Statistische Analyse des ENSO- und Vulkanismus-Signals in Klima-Zeitreihen. Diplomarbeit, Inst. f. Meteorologie u. Geophysik, Universität Frankfurt, 1998.

[18] A. Walter, M. Denhard, and C.-D. Schönwiese. Simulation of Global and Hemispheric Temperature Variations and Signal Detection Studies using Neural Networks. *Meteorologische Zeitschrift*, N.F.7:171–180, 1998.

[19] A. Werner. Die Nord-Atlantik-Oszillation und ihre Auswirkungen auf Europa. Diplomarbeit, Inst. f. Meteorologie u. Geophysik, Universität Frankfurt, 1999.